

1
2
3
4
5
6
7
8
9
10
11
12
13
14
15
16
17

Convective transport of very-short-lived bromocarbons to the stratosphere

Qing Liang^{1,2}, Elliot Atlas³, Donald Blake⁴, Marcel Dorf^{5,6}, Klaus Pfeilsticker⁵, Sue Schauffler⁷

[1] {NASA Goddard Space Flight Center, Atmospheric Chemistry and Dynamics, Greenbelt, MD, USA}

[2] {Universities Space Research Association, GESTAR, Columbia, MD, USA}

[3] {University of Miami, 4600 Rickenbacker Causeway, Miami, FL 33149, USA}

[4] {University of California, 570 Rowland Hall, Irvine, CA 92697, USA}

[5] {Institut für Umweltphysik, University of Heidelberg, Heidelberg, Germany}

[6] {Now at Max-Planck-Institut für Chemie, Mainz, Germany}

[7] {Earth Observing Laboratory, NCAR, Boulder, CO, USA}

Correspondence to: Q. Liang (Qing.Liang@nasa.gov)

17 **Abstract.** We use the NASA GEOS Chemistry Climate Model (GEOSCCM) to quantify the
18 contribution of two most important brominated very short-lived substances (VSLs), bromoform
19 (CHBr_3) and dibromomethane (CH_2Br_2), to stratospheric bromine and its sensitivity to
20 convection strength. Model simulations suggest that the most active transport of VSLs from the
21 marine boundary layer through the tropopause occurs over the tropical Indian Ocean, the tropical
22 western Pacific, and off the Pacific coast of Mexico. Together, convective lofting of CHBr_3 and
23 CH_2Br_2 and their degradation products supplies ~ 8 ppt total bromine to the base of the Tropical
24 Tropopause Layer (TTL, ~ 150 hPa), similar to the amount of VSLs organic bromine available in
25 the marine boundary layer (~ 7.8 - 8.4 ppt) in the above active convective lofting regions. Of the
26 total ~ 8 ppt VSLs bromine that enters the base of TTL at ~ 150 hPa, half is in the form of organic
27 source gases and half as inorganic product gases. Only a small portion ($<10\%$) of the VSLs-
28 originated bromine is removed via wet scavenging in the TTL before reaching the lower
29 stratosphere. On global and annual average, CHBr_3 and CH_2Br_2 , together, contribute ~ 7.7 pptv
30 to the present-day inorganic bromine in the stratosphere. However, varying model deep
31 convection strength between maximum (strongest) and minimum (weakest) convection
32 conditions can introduce a ~ 2.6 pptv uncertainty in the contribution of VSLs to inorganic
33 bromine in the stratosphere ($\text{Br}_y^{\text{VSLs}}$). Contrary to the conventional wisdom, minimum
34 convection condition leads to a larger $\text{Br}_y^{\text{VSLs}}$ as the reduced scavenging in soluble product gases,
35 thus a significant increase in product gas injection (2-3 ppt), greatly exceeds the relative minor
36 decrease in source gas injection (a few 10ths ppt).

37

38 **1. Introduction**

39 Very short-lived (VSL) bromocarbons originate mostly from ocean biogenic sources, and
40 when transported into the stratosphere, they exert a significant impact on the bromine budget and
41 stratospheric ozone depletion (Kurylo and Rodriguez, 1999; Sturges et al., 2000). Recent years
42 have seen significant progress in modeling efforts to quantify the contribution of brominated
43 VSL substances (VSLs) to stratospheric inorganic bromine ($\text{Br}_y^{\text{VSLs}}$) (e.g. Warwick et al., 2006;
44 Liang et al., 2010; Aschmann et al., 2011; Aschmann and Sinnhuber, 2013; Hossaini et al.,
45 2012a, 2012b, 2013). These modeling studies suggest that brominated VSLs contribute 4.8-7 ppt
46 to reactive stratospheric bromine, within the 1-8 ppt estimate range from satellite and balloon-
47 borne observations (WMO 2011; Sinnhuber et al., 2005; Sioris et al., 2006; Dorf et al., 2006a,
48 2008; Salawitch et al., 2010).

49 The most important VSLs pathway to the stratosphere is via convective lofting through the
50 tropical tropopause layer (TTL). Atmospheric chemistry and transport of brominated VSLs
51 involves the coupling of various complex processes, e.g. highly un-uniform ocean emissions,
52 convective transport of source gases and product gases, as well as wet scavenging of soluble
53 product gases. An accurate modeling representation of these processes remains a challenging
54 task. Modeling of these processes in general requires some extent of simplified assumptions
55 and/or parameterizations, which may differ greatly from one model study to another. These
56 differences have led to significant differences in the modeled $\text{Br}_y^{\text{VSLs}}$ estimates. For example, a
57 recent model study by Hossaini et al. (2013) found that modeled $\text{Br}_y^{\text{VSLs}}$ could vary by a factor of
58 2 when using four recently published emission inventories (Liang et al., 2010; Pyle et al., 2011;
59 Ordóñez et al., 2012; Ziska et al., 2013). In general, model studies agree relatively well on
60 source gas injection (SGI), suggesting about $\sim 50\%$ of bromoform (CHBr_3) and $\sim 90\%$ of
61 dibromomethane (CH_2Br_2) can reach the stratosphere through SGI (e.g. Dvortsov et al., 1999;
62 Nielsen and Douglass, 2001; Aschmann et al., 2011; Hossaini et al., 2010, 2012a). However,

63 modeled contribution on product gas injection (PGI) is highly uncertain depending on how wet
64 scavenging is implemented. Many early model studies assume a uniform washout lifetime
65 against wet scavenging (e.g. Dvortsov et al., 1999; Nielsen and Douglass, 2001; Hossaini et al.,
66 2010; Aschmann et al., 2009), which was inadequate and lead to an underestimate in modeled
67 Br_y^{VLS} (Hossaini et al., 2012a; Aschmann et al., 2011). A recent study by Aschmann and
68 Sinnhuber (2013) shows that treating Br_y^{VLS} as a single soluble tracer (e.g. Liang et al., 2010)
69 can also lead to an underestimate. They found that Br_y^{VLS} increased from 3.4 ppt to 5 ppt when
70 switching from an idealized setup with a single soluble inorganic bromine tracer to a full
71 chemistry scheme. Thus, an accurate modeling of transport and wet scavenging of PGI seems to
72 be the key in narrowing the uncertainty of model estimate of Br_y^{VLS} .

73 Understanding how the contribution of VLS to stratospheric bromine varies with
74 convection strength has significant climate implications. A recent modeling analysis by Hossaini
75 et al (2012b) suggests that VLS SGI increases from ~ 1.7 ppt in 2000 to ~ 2.0 - 2.7 ppt in 2100
76 using the Intergovernmental Panel on Climate Change (IPCC) representative concentration
77 pathways (RCPs) scenarios, as the future simulations feature stronger tropical deep convection
78 transport to the lower stratosphere. On the other hand, the overall response of Br_y^{VLS} to
79 convection strength is somewhat murky. Earlier studies deploying a uniform washout lifetime
80 found different washout rates result a significant range in the contribution of CHBr_3 to Br_y , 0.5-3
81 ppt in Sinnhuber and Folkins (2006) and 1.6-3 ppt in Aschmann et al., (2011). Liang et al.
82 (2010) which deploys explicit wet scavenging in convective updrafts found that convective
83 scavenging only accounts for ~ 0.2 ppt difference in modeled Br_y^{VLS} . Similar results were
84 reported in Aschmann et al. (2011), who showed while SGI is highly correlated with convective
85 activity, the impact on total stratospheric bromine in a full chemistry scheme is nearly insensitive
86 to dehydration, likely due to convection dilution and increased scavenging.

87 In this study, we use a 3-dimensional Chemistry Climate Model with fully interactive CHBr_3
88 and CH_2Br_2 , the two most important brominated VLS, to better understand how VLS and their
89 degradation products enter the stratosphere. We will also test the uncertainty in modeled Br_y^{VLS}
90 due to varying strength in convection and scavenging.

91

92 **2. Model and Simulations**

93 **2.1 Model Description**

94 We conduct model simulations using the NASA GEOS Chemistry Climate Model
95 (GEOSCCM) Version 2, which couples the GEOS-5 GCM (Reinecker et al., 2008) with a
96 stratospheric chemistry module. Model simulations have a horizontal resolution of $2.5^\circ \times 2^\circ$
97 (longitude by latitude) with 72 vertical layers from surface to 0.01 hPa. The GEOS-5 model uses
98 a flux-form semi-Lagrangian dynamical core (Lin, 2004) and the Relaxed Arakawa Schubert
99 (RAS) parameterization for convection (Moorthi and Suarez, 1992). The GEOS-5 moist
100 processes are represented using a convective parameterization and prognostic cloud scheme.

101 The GEOSCCM V2 stratospheric chemistry module includes all important gas phase
102 stratospheric reactions as described in Douglass and Kawa (1999), and chemical calculations are
103 carried out above the 27th eta layer (approximately 350 hPa on global average). All chemical
104 kinetics and photolysis rates are calculated following JPL 2010 (Sander et al., 2011). We modify
105 the standard V2 chemistry scheme to include CHBr_3 and CH_2Br_2 , both are interactive with the
106 full stratospheric chemistry scheme. The two organic source gases are released at the ocean
107 surface following the geographically resolved emission distribution described in Liang et al.
108 (2010) and are destroyed in the atmosphere via photolysis and reaction with the hydroxyl radical

109 (OH). OH above ~350 hPa is calculated online in the stratospheric chemistry module. OH in the
110 lowest 26 layers (troposphere) is relaxed to a monthly mean climatological fields documented in
111 Spivakovsky et al. (2000). Global annual mean OH from Spivakovsky et al. (2000) is 1.16×10^6
112 molecules cm^{-3} , yielding an atmospheric methyl chloroform (CH_3CCl_3) lifetime of ~5.5 years. In
113 most of the troposphere, only simple bromine chemistry is considered which partitions 80% of
114 inorganic bromine products into HBr and the remaining 20% as HOBr, ratios adopted from Yang
115 et al. (2005). Above the 27th eta layer (~350 hPa), bromine from CHBr_3 and CH_2Br_2 degradation
116 is released as Br and interacts fully with stratospheric chemistry. Compare to the idealized case
117 in Liang et al. (2010) that tracks the atmospheric transport of $\text{Br}_y^{\text{VLSL}}$ in a single highly soluble
118 tracer, in this experiment, we deploy a detailed speciation of $\text{Br}_y^{\text{VLSL}}$ in both soluble forms (HBr,
119 HOBr, and BrONO_2) and insoluble forms (Br, BrO, BrCl) in the fully interactive stratospheric
120 chemistry scheme in the TTL and stratosphere. Although BrONO_2 is not produced in the
121 troposphere in the current simple chemistry scheme, BrONO_2 produced in the stratosphere is
122 allowed to transport to lower altitudes via large-scale descent. A previous detailed tropospheric
123 chemistry model study using the Harvard GEOS-Chem model and VLSL emissions from Liang
124 et al (2010) shows a small fraction of Br_y exists as BrO (0.1-0.2 ppt) below 10 km in the tropics
125 (Parrella et al., 2012). However, the impact of the absence of this tropospheric BrO on
126 stratospheric bromine is likely small. No heterogeneous chemistry for VLSL is included in our
127 simulations, but results from Aschmann and Sinnhuber (2013) suggest that the impact of
128 heterogeneous chemistry is minor and the inclusion of heterogeneous activation prevents loss in
129 scavenging and can increase $\text{Br}_y^{\text{VLSL}}$ by 10%. While heterogeneous chemistry can shift Br_y
130 partition and increase HBr up to 4 times between 12-18 km in the tropics (Aschmann et al,
131 2011), the absence of heterogeneous chemistry in GEOSCCM is likely to have only a small
132 impact on $\text{Br}_y^{\text{VLSL}}$ since the model HBr is present at very low abundance during daytime when the
133 majority of convective scavenging take place (see section 3.1 and Figure 4) and the overall
134 convective scavenging in the TTL is rather inefficient (see section 3.2).

135 The wet scavenging of the soluble inorganic bromine are the same as that detailed in Liang et
136 al. (2010). It includes scavenging in rainout (in-cloud precipitation) and washout (below-cloud
137 precipitation) in both large-scale precipitation (Giorgi and Chameides, 1986) and deep
138 convective updrafts (Balkanski et al., 1993). We assume high solubility for all three inorganic
139 bromine reservoir species, HBr, HOBr, and BrONO_2 . At each time step, we follow the Giorgi
140 and Chameides (1986) parameterization to compute the wet scavenging using the GEOS-5 model
141 calculated large-scale and convective precipitation rates and the parameterized fraction of grid
142 square area, F , that actually experience precipitation (Balkanski et al., 1993). Wet scavenging
143 occurs only when air temperature is above 258K, following Giorgi and Chameides (1986).
144 Previous studies using the Giorgi and Chameides (1986) parameterization showed that, for large-
145 scale precipitation, the global mean F is about 2.5% for all grid boxes and the median value is
146 10%, with values exceeding 40% in ~10% of the grid boxes (Balkanski et al., 1993; Liu et al.,
147 2001). The global mean F for convective precipitation is much smaller, only 0.4% (Liu et al.,
148 2001). When evaporation occurs during large-scale and convective transport, the corresponding
149 fraction of the dissolved inorganic bromine is released back to the atmosphere. This wet
150 scavenging scheme has been applied in many atmospheric modeling studies of soluble trace
151 gases and aerosols, e.g. ^{210}Pb , ^7Be , sulfate, sea salt, dust, and the simulated concentrations
152 compare well with surface observations at many observation sites around the globe (e.g.
153 Balkanski et al., 1993; Chin et al., 2000; Ginoux et al., 2001; Liu et al., 2001).

154 In this study, we present results from two 51-year simulations between 1960-2010, one with
155 brominated VLS chemistry (R_{VLS}) and one without (R_{BASE}), to examine troposphere to
156 stratosphere transport (TST) of VLS and their contribution to stratospheric bromine. It takes a
157 considerable long time (~ 15 years) for the full impact of VLS to reach the upper stratosphere,
158 thus the first 16 years are considered as spin-up. A full model evaluation and discussion of the
159 impact of VLS on stratospheric ozone are presented in a separate paper, currently in
160 preparation. For this study, we focus on model results from the last 10 years of the two
161 simulations.

162 **2.2 Convection Sensitivity Simulations**

163 To quantify the uncertainty in Br_y^{VLS} due to changes in convection strength, we conduct two
164 sensitivity simulations from 1980 to 2010 to represent minimum convection (R_{MINCNV}) and
165 maximum convection (R_{MAXCNV}) conditions by varying five convective parameters in RAS that
166 impact the strength of deep convection, clouds, convective condensate and re-evaporation (Ott et
167 al., 2009; 2011). These five convective parameters are RASAL1 and RASAL2 (regulates the
168 strength and vertical profile of the relaxation time scale for deep convection), ACRITFAC (used
169 to compute the critical value of the cloud work function which determines the initiation of
170 convection), BASE_EVAP_FAC (regulates the amount of rain evaporated into the environment
171 below the cloud base), and AUTO_CN (used to calculate the autoconversion of convective
172 condensate). These five are identified as the most strongly influencing out of the total 16
173 parameters examined using a large number of “Monte Carlo” type simulations and ensemble
174 simulations in both a Single-Column Model as well as the GEOS-5 GCM (Ott et al., 2011). In
175 the two sensitivity simulations, the five parameters are varied to produce the strongest
176 (MAXCNV) and the weakest (MINCNV) representations of convection considered reasonable.
177 In general, compared to the minimum convection condition, the maximum convection condition
178 yields significantly large increases in shallow convection below 5 km and $\sim 20\text{-}30\%$ stronger
179 vertical mass flux and more horizontal divergence between 12.5-16.5 km (Ott et al., 2011). The
180 values used for the five convective parameters for the minimum and maximum conditions have
181 been tested extensively in the previous ensemble analysis that they produce reasonable
182 precipitation patterns when compared with data from the Global Precipitation Climatology
183 Project (GPCP) that were compiled from satellite and rain gauge observations (Ott et al., 2011).
184 The correlation coefficients between the standard run, MAXCNV and MINCNV simulations and
185 the GPCP data sets are 0.65, 0.64, 0.62, respectively (Ott et al., 2011).

186 We aim to use these minimum and maximum conditions to bound the range of uncertainty
187 that can be introduced due to variations in the strength of convection and wet scavenging.
188

189 **3. Results**

190 **3.1 The Contribution of VLS to Stratospheric Bromine**

191 The simulated CHBr_3 and CH_2Br_2 have been evaluated extensively in Liang et al. (2010) and
192 compares well with aircraft and surface observations in their atmospheric distribution,
193 geographically and vertically, as well as the associated seasonality. Here we present a summary
194 comparison of observed and modeled CHBr_3 in the troposphere for 30-60°S, 30°S-30°N, 30-
195 60°N, and 60-90°N latitude bands (Figure 1). The observed profiles are compiled using Whole
196 Air Sampler canister measurements (Schaufler et al., 1999; Blake et al., 2003) from eight NASA
197 aircraft missions, as detailed in Liang et al. (2010), and averaged within each latitude band at 1-
198 km vertical interval. The comparison clearly shows that the model captures well the source gas
199 concentrations and vertical gradients in the tropics, mid and high latitudes in both hemispheres.

200 Figure 2 shows a comparison of our simulated BrO with balloon measurements from the
201 LPMA (Limb Profile Monitor of the Atmosphere) / DOAS (Differential Optical Absorption
202 Spectroscopy) at Teresina (5.1°S), Aire sur l'Adour (43.7°N), and Kiruna (67.9°N) collected
203 between 2003-2005 (Dorf et al., 2006a, 2006b, 2008; Rozanov et al., 2011). The lower levels of
204 BrO from R_{BASE} in comparison to the measurements indicate the essential role of VLS in
205 completing the stratospheric bromine budget. With VLS, the GEOSCCM model simulates well
206 the observed BrO at all sampled locations in the tropics, mid and high latitudes. Currently the
207 GEOSCCM does not include the remaining 3 of the 5 major brominated VLS, CH_2BrCl ,
208 CHBr_2Cl and CHBrCl_2 (lifetimes between 70-150 days). Assuming a total tropospheric
209 abundance of 1 ppt of these three VLS and $\sim 90\%$ (value for CH_2Br_2) of the source gases
210 survive the TST to the stratosphere, this adds ~ 0.9 ppt to the current model estimate of
211 stratospheric Br_y of ~ 24 ppt. With the current model BrO/Br_y ratio, such an increase will lead to
212 an increase in BrO in the stratosphere up to 0.6 ppt (not shown). This results a better agreement
213 with the DOAS BrO measurements in Teresina and Aire sur l'Adour and reasonable agreement
214 at Kiruna, considering the large spatial variability in BrO in the high latitudes and rather
215 localized balloon measurements. Since the model is running freely by specifying only surface
216 source gas emissions, the fact that the model simulates well the observed concentrations for both
217 the source gases and BrO suggests that the model presents a credible representation of
218 stratospheric bromine chemistry.

219 Comparing results from the R_{VLS} and R_{BASE} runs (Figure 3), we find that the inclusion of
220 CHBr_3 and CH_2Br_2 adds a uniform ~ 7.7 ppt Br_y throughout most of the stratosphere. The current
221 Br_y^{VLS} estimate is 55% higher than our previous estimate of ~ 5 ppt (Liang et al., 2010) and ~ 6
222 ppt estimate in Hossaini et al. (2013), though the latter two are driven by the same VLS
223 emissions. Compared to the idealized case in Liang et al. (2010) that tracks Br_y^{VLS} in a single
224 highly soluble tracer, Br_y^{VLS} in this study is present in the fully interactive stratospheric
225 chemistry scheme in both soluble forms (HBr , HOBr , and BrONO_2) and insoluble forms (Br ,
226 BrO , BrCl) in the TTL. The ratio of insoluble and soluble Br_y varies with time of the day as well
227 as altitude and location. Figure 4 shows the contrast of model inorganic bromine speciation in
228 the tropics between daytime and nighttime. In the TTL region, at daytime, when most convective
229 lofting occurs, the majority of Br_y exists as insoluble Br and BrO (Figure 4a), therefore greatly
230 increases the amount of Br_y^{VLS} that survives wet scavenging during the TST and ultimately
231 reaches the stratosphere. The increase from ~ 5 ppt to ~ 7.7 ppt when switching from an idealized
232 case to fully interactive stratospheric chemistry is consistent with results from Aschmann and
233 Sinnhuber (2013), who found that Br_y^{VLS} increased from 3.4 ppt to 5 ppt when switching from
234 an idealized setup with a single soluble inorganic bromine tracer to a full chemistry scheme. The
235 different estimates between Hossaini et al. (2013) and this work are likely due to how the ratio of
236 soluble and insoluble inorganic bromine is determined inside the two models. Compared to this
237 work which partitions inorganic bromine in its various forms based on chemical reaction rates,
238 Hossaini et al. (2013) used a mean altitude-dependent $\text{HBr}:\text{Br}_y$ ratio. This likely leads to an
239 excessive washout of Br_y^{VLS} as during daytime when most of the convective lofting occurs, the
240 majority of the inorganic bromine exists as insoluble Br and BrO . This suggests that a close
241 approximate of soluble and insoluble inorganic product gases and the associated diurnal variation
242 are critical to accurately quantify the contribution of VLS to stratospheric halogen in VLS
243 modeling.

244 A recent study by Kreycky et al. (2013), using balloon borne DOAS BrO measurements over
245 Kiruna (67.9°N, 22.1°E), suggests that the ratio of $J(\text{BrONO}_2)/k_{\text{BrO}+\text{NO}_2}$ should be a factor of 1.7

246 larger than the JPL 2010 recommendations and is likely to shift more BrONO₂ into BrO.
247 However, this result will have only a small impact on our Br_y^{VLSL} estimates. Currently, BrONO₂
248 only accounts for ~0.5 ppt of the total Br_y^{VLSL} in the TTL during daytime. In addition, convective
249 scavenging of the inorganic bromine in the TTL is not an efficient removal process (section 3.2).
250 Increasing the ratio of J(BrONO₂)/k_{BrO+NO₂} in the model will shift Br_y^{VLSL} partition from BrONO₂
251 to BrO, which in turn will result an increase in Br_y^{VLSL} due to less BrONO₂ scavenging. However,
252 this increase will be small (at most a few tenths ppt).

253 3.2 Troposphere-to-Stratosphere Transport of VLSL

254 We use the simulated monthly mean CHBr₃ distribution on the 355 K potential temperature
255 surface (just below TTL) to show important tropical regions where active TST initiates (Figure
256 5). Theoretically, trace gas distribution on the 365 K surface should be more indicative of TST
257 as 365 K marks the zero radiative heating and air mass elevated above this level can enter the
258 lower stratosphere through slow radiative ascent (e.g. Gettelman and Forster, 2002; Fueglistaler
259 et al., 2009). However, it is difficult to identify active TST regions on the 365 K map (not
260 shown) as a significant portion of CHBr₃ is converted to product gases. This is not surprising for
261 a short-lived compound with lifetime ~ 26 days (WMO 2011) while on average it takes about 10
262 days for air to transport by ±10 K (Fueglistaler et al., 2004; Levine et al., 2007). Compared to
263 CHBr₃, it is much more difficult to identify active TST regions on a CH₂Br₂ map, as CH₂Br₂
264 distribution appears more zonal with a smaller meridional gradient due to a longer lifetime, ~
265 120 days (WMO 2011) and up to ~ 450 days locally in the TTL (Hossaini et al., 2010), and thus
266 more mixing with the surrounding background air (not shown). The 355K CHBr₃ map shows
267 three active regions that can efficiently deliver VLSL to the base of TTL: 1) the tropical Indian
268 Ocean, 2) the tropical western Pacific, and 3) off the Pacific coast of Mexico (Figure 5). There is
269 significant seasonality associated with each entry region. The Indian Ocean appears as the most
270 active region for the TST of CHBr₃ and occurs all year long with a maximum in boreal winter
271 (DJF). Lofting in the tropical western Pacific reaches its maximum in boreal summer (JJA),
272 while the TST off the Mexico coast occurs mostly in boreal summer (JJA) and fall (SON). The
273 importance of convective lofting in the Western Pacific warm pool in TST has been noted in
274 many previous studies (e.g. Hatsushika and Yamazaki, 2003; Fueglistaler et al., 2004; Aschmann
275 et al., 2009; Hossaini et al., 2012a; Ashfold et al., 2012) with several others suggesting that the
276 Indian Ocean is also an important region in the TST of VLSL (Levine et al., 2007, 2008; Brioude
277 et al., 2010; Hoyle et al., 2011).

278 We show in Figure 6 the vertical profiles of organic source gases (CH₂Br₂×2, CHBr₃×3) and
279 inorganic product gases in the three critical convective lofting regions to illustrate the transport
280 and wet scavenging of the brominated VLSL during the TST and the relative importance of SGI
281 vs. PGI. Although tropospheric Br_y are assumed highly soluble, only a fraction of the grid boxes
282 and a fractional area of the precipitating grid boxes actually experiencing precipitation and
283 scavenging. On average, of all inorganic bromine (~4 ppt) produced from CHBr₃ and CH₂Br₂ in
284 the tropical troposphere, about 50% (~2 ppt) is removed below 500 hPa, mainly by large-scale
285 precipitation (Liang et al., 2010), with an additional few tenths ppt scavenged in the upper
286 troposphere. Together, ~1.5 ppt of HBr and HOBr survive large-scale and convective
287 scavenging and remain in the tropical upper troposphere. Br, BrO, and BrONO₂ produced from
288 CHBr₃ and CH₂Br₂ degradation in the tropical upper troposphere adds an additional ~2 ppt to
289 Br_y^{VLSL}. Over the tropical Indian Ocean, on annual average, the mixing ratio of total bromine
290 from VLSL (organic + inorganic) at 150 hPa (~355K) is ~8.5 ppt, the same as its surface
291 abundance (~8.5 ppt). This implies convective lofting in this region is so efficient that the

292 amount of VSL bromine that enters the base of TTL is set by the concentration at the marine
293 boundary layer. As air ascend to higher altitudes, a small portion of $\text{Br}_y^{\text{VSLs}}$ (~ 0.8 ppt, 10%) is
294 gradually removed from the atmosphere via wet scavenging until reaching a constant 7.7 ppt
295 above 10 hPa. Results from the tropical western Pacific and off the coast of Mexico are similar,
296 with a smaller surface abundance of organic bromine (7.8~8.1 ppt) and slightly less washout
297 around 100 hPa. The global averaged total bromine from VSLS (Br^{VSLs}) profile shows a
298 maximum value of ~ 8 ppt at ~ 100 hPa. To supply this amount of Br^{VSLs} to the lower stratosphere,
299 transport from the marine boundary layer has to initiate from tropical regions where active
300 convective lofting is co-located with high surface concentrations, where the collective CHBr_3
301 and CH_2Br_2 abundance exceeds 8 ppt Br.

302 Mapping streamlines on top of the VSLS organic bromine distribution in the tropics clearly
303 illustrates the importance of co-location of deep convection with high surface concentration
304 regions (Figure 7). Among the three ascending branches of the Walker circulation (Webster
305 1983), while ascent in the tropical western Pacific penetrates deepest into the TTL, ascent in the
306 Indian Ocean is capable in delivering more VSLS bromine to the base of TTL due to higher
307 surface concentrations. The surface abundance of VSLS bromine is largely dependent on the
308 emission distribution used. Liang et al. (2010) assumed uniform zonal emission strength across
309 all longitudes, but the rate of bromocarbon emissions for the coastal regions per unit area are
310 much higher than that in the open oceans. In the tropics, the prevailing surface easterly trade
311 winds tend to bring recent emissions of CHBr_3 from the adjacent Indonesian coastal regions
312 while the tropical western Pacific Ocean sees recent emissions of CHBr_3 from the open ocean.
313 Therefore, the surface concentrations are higher in the Indian Ocean than the tropical western
314 Pacific. However, it is important to point out that only a few surface observation constraints from
315 the tropical western Pacific and none from the tropical Indian Ocean were available to derive the
316 Liang et al., (2010) emission scenario. Hossaini et al. (2013) conducted a recent model study
317 comparing four independent brominated VSLS emission estimates. Of all four emission
318 inventories examined (Liang et al., 2010; Pyle et al., 2011; Ordóñez et al., 2012; Ziska et al.,
319 2013), modeled CHBr_3 and CH_2Br_2 concentrations using the emission estimates from Liang et al.
320 (2010) compare very well against tropical observations from multiple years of National Oceanic
321 and Atmospheric Administration/Earth System Research Laboratory (NOAA/ESRL) surface
322 flask measurements. The global mean model biases (model – observations) are -0.25 ppt for
323 CHBr_3 (ranging from $+0.12$ ppt in the tropics to -0.65 ppt in the northern high latitudes) and $-$
324 0.02 ppt for CH_2Br_2 (ranging from $+0.14$ ppt in the tropics to -0.11 ppt in the northern and
325 southern high latitudes). Comparison with the HIAPER Pole-to-Pole Observations (HIPPO)
326 measurements between 2009–2011 supported by the National Science Foundation (NSF) yields
327 even better agreement, with little biases in global mean CHBr_3 ($\Delta_{\text{model-obs}} = +0.04$ ppt) and
328 CH_2Br_2 ($\Delta_{\text{model-obs}} = -0.01$ ppt). The modeled biases for each latitude band are also small, $-0.16 -$
329 $+0.30$ ppt for CHBr_3 and $-0.10 - +0.12$ ppt for CH_2Br_2 . When compared against the aircraft
330 measurements collected in the tropical western Pacific during the Stratospheric Ozone: Halogen
331 Impacts in a Varying Atmosphere (SHIVA) campaign, Liang et al. (2010) yields the best CH_2Br_2
332 (mean bias of $+0.2$ ppt compared with observations), compared to the other three emissions, but
333 the simulated CHBr_3 is $\sim +0.76$ ppt too high on average. Note the high bias in modeled CHBr_3
334 in the tropical western Pacific will likely lead to a high bias in the model $\text{Br}_y^{\text{VSLs}}$, although the
335 lofting in Indian Ocean seems to be more critical in determining the total amount of VSLS
336 bromine in the lower stratosphere in this study. The model simulated high concentration of
337 brominated VSLS over the Indian Ocean is yet to be evaluated when more surface observations

338 become available and the importance of the Indian Ocean in delivering higher amounts of VSLs
339 bromine into the TTL needs to be assessed. The simulated high surface concentrations of CHBr_3
340 and CH_2Br_2 near tropical Central America were validated with the NASA TC⁴ and INTEX-B
341 measurements (Liang et al., 2010). This region, compared to the above two, is much less
342 efficient in delivering VSLs bromine into the TTL due to the relatively weaker ascent.
343 However, this ascending branch can be important in particular seasons and in individual years as
344 the Walker circulation moves in the east-west direction between different phases of the El Niño
345 Southern Oscillation (ENSO). For example, using trajectory calculations, Levine et al. (2008)
346 found a clear shift in the TTL origin of air parcels from the tropical western Pacific and
347 Indonesia to those from the Eastern Pacific and South America in El Niño years.

348 Of the total VSLs bromine that enters the base of TTL, about half (~4 ppt) is in the form of
349 inorganic product gases (Figure 6) despite our simple assumption that all inorganic bromine
350 reservoir species are highly soluble and all inorganic bromine produced below 350 hPa are
351 partitioned into the soluble forms - HBr and HOBr. A commonly adopted approach in many
352 previous modeling studies is to prescribe the VSLs concentration at the base of TTL with
353 observed organic source gas mixing ratios in the upper troposphere and tracks the subsequent
354 chemistry and transport (e.g. Sinnhuber and Folkins, 2006; Aschmann et al. 2011, Aschmann and
355 Sinnhuber, 2013). Our result implies that $\text{Br}_y^{\text{VSLs}}$ estimate from such approach is not complete as
356 it misses an important component associated with PGI, which is as large as SGI at the base of
357 TTL in our model simulation. A second implication of this result is that if we were to use
358 measurements from the TTL region to quantify the contribution of VSLs to stratospheric
359 bromine, it is necessary to make measurements of both organic and inorganic forms to fully
360 account for the impact of VSLs on the atmospheric bromine budget.

361 3.3 The Impact of Convection Strength

362 We examine the difference between the two convection sensitivity simulations, R_{MINCNV} and
363 R_{MAXRUN} , to illustrate the impact of deep convection on $\text{Br}_y^{\text{VSLs}}$ (Figure 8). Difference between
364 these two simulations ($R_{\text{MINCNV}} - R_{\text{MAXRUN}}$) suggests that in regions that mattered most (the three
365 tropical convection centers), surprisingly, the minimum convection condition is more favorable
366 for the TST of VSLs. While weaker convection slightly decreases SGI (a few tenths ppt), PGI
367 increases significantly (2-3 ppt) due to less scavenging under minimum convection condition.
368 TST of the longer-lived CH_2Br_2 is less sensitive to convection strength compared to that of
369 CHBr_3 because of its longer lifetime. The significant increase in CHBr_3 and CH_2Br_2 in the mid-
370 latitude bands under minimum convection mainly reflects the compensating responses in large-
371 scale descent in a general circulation model as a result of changing convection strength (Ott et
372 al., 2011). The decrease of the descent does not impact TST of VSLs. Aschmann et al. (2011)
373 found a qualitatively similar behavior for changes of VSLs SGI and PGI under El Niño vs. La
374 Niña conditions - while SGI increased slightly under enhanced deep convection, the sum of SGI
375 and PGI decreased. However, the net decrease in the $\text{Br}_y^{\text{VSLs}}$ (<0.5 ppt) due to changes in
376 convection strength between El Niño vs. La Niña conditions reported in Aschmann et al. (2011)
377 is much smaller than our results above, most likely due to a much higher $\text{Br}_y^{\text{VSLs}}$ abundance in
378 the TTL in this work.

379 Globally, the differences in convection strength and wet scavenging introduce a ~2.6 ppt
380 uncertainty in $\text{Br}_y^{\text{VSLs}}$ (~6.5 ppt in R_{MAXRUN} and ~9.1 ppt in R_{MINRUN}) (Figure 3). Although these
381 two simulations represent the two extreme parameterization conditions within reasonable range,
382 BrO from both simulations still falls within the uncertainty range of the DOAS balloon
383 observations of ± 2.5 ppt (Figure 2, Dorf et al., 2006b).

384
385
386
387
388
389
390
391
392
393
394
395
396
397
398
399
400
401
402
403
404
405
406
407
408
409
410
411
412
413
414
415
416
417
418
419
420
421
422
423
424
425
426
427
428
429

4. Conclusions

We use the NASA Goddard 3-D Chemistry Climate Model, GEOSCCM, to quantify the contribution of brominated very short-lived substances (VSLS) to reactive stratospheric bromine and to test its sensitivity to the strength of deep convection and the associated scavenging.

The inclusion of CHBr_3 and CH_2Br_2 in a fully interactive stratospheric chemistry module deployed in the TTL and the stratosphere adds ~ 7.7 pptv to the present-day stratospheric inorganic bromine. The most active transport of VSLS from the marine boundary layer through the tropical tropopause layer (TTL) occurs where high surface concentrations of VSLS co-locate with deep convection centers: 1) the tropical Indian Ocean, 2) the tropical western Pacific warm pool, and 3) off the Pacific coast of Mexico. On annual average, almost all VSLS-originated bromine available in the marine boundary layer (~ 7.8 - 8.4 ppt) at these active convective lofting regions enters the TTL, half in the form of source gas injection (SGI) and half in the form of product gas injection (PGI). After lofting above 150 hPa ($\sim 355\text{K}$), the majority of the VSLS-originated bromine survives TST and reaches the lower stratosphere, with only a small portion (~ 0.8 ppt, 10%) removed by wet scavenging. Our model results point to a clear need for more surface measurements in the active VSLS lofting regions, in particular the tropical Indian Ocean and the tropical western Pacific, for improved emissions estimate as well as a better quantification of how much VSLS bromine is available before ultimately enters the stratosphere through the TTL.

Our current estimate of the contribution of CHBr_3 and CH_2Br_2 to stratospheric bromine ($\text{Br}_y^{\text{VSLS}}$) is higher than previous modeling estimates, mainly reflecting the differences in how transport and wet scavenging of product gases are treated in different models (Hossaini et al., 2012a; Aschmann and Sinnhuber, 2013). Interestingly, even though the models are driven with same emission estimates (Liang et al., 2010; Hossaini et al, 2013) and/or with similar source gas abundance at the base of TTL (Aschmann et al. 2011; Aschmann and Sinnhuber, 2013), this study still yields higher $\text{Br}_y^{\text{VSLS}}$ for two main reasons. Modeling VSLS and their degradation products in a full stratospheric chemistry scheme in the TTL and stratosphere leads to a better representation of the partition between soluble and insoluble product gases and the associated diurnal variation, both are critical in an accurate $\text{Br}_y^{\text{VSLS}}$ estimate. Secondly, tracking PGI from the free troposphere to the base of TTL, which is as large as SGI at the base of TTL in our model simulation, is also important. This was not included in many earlier model studies (e.g. Aschmann et al. 2011; Aschmann and Sinnhuber, 2013), thus implying a missing component in these earlier model VSLS contribution estimates.

Differences in model deep convection strength can introduce $\sim 30\%$ (6.6 ppt - 9.2 ppt) uncertainty in simulated $\text{Br}_y^{\text{VSLS}}$ within the same convection scheme. It is important to point out that this uncertainty is likely larger among different models or a same model but different versions when different convective parameterizations are used.

Contrary to conventional wisdom that the VSLS impact on stratospheric bromine is larger under more intense deep convection, our simulations suggest that minimum convection condition is favorable for TST of VSLS due to reduced scavenging of soluble product gases under weaker convection. The impact of convection strength on PGI greatly outweighs the impact on SGI with the change in PGI \sim ten times larger than that of SGI.

Acknowledgements. Funding for this research is from the NNX11AN71G project supported by the NASA ACMAP program. Funding for the DOAS team are from the German

430 Ministry of Economy (BMWi) (50EE0840), the European Space Agency (ESA-ESRIN: no.
431 RFQ/3-12092/07/I-OL) and the Deutsche Forschungsgemeinschaft, DFG (grants PF-384/5-1
432 and 384/5-1 and PF384/9-1/2), as well as Additional funding from the EU projects Reconcile
433 (FP7-ENV-2008-1-226365) and SHIVA (FP7-ENV-2007-1-226224). We thank Björn-Martin
434 Sinnhuber and the other anonymous reviewer for their great and constructive comments.
435

435 **References**

- 436 Aschmann, J., Sinnhuber, B.-M., Atlas, E. L., and Schauffler, S. M.: Modeling the transport of
437 very short-lived substances into the tropical upper troposphere and lower stratosphere,
438 *Atmos. Chem. Phys.*, 9, 9237–9247, doi:10.5194/acp-9-9237-2009, 2009.
- 439 Aschmann, J., Sinnhuber, B.-M., Chipperfield, M. P., and Hossaini, R.: Impact of deep
440 convection and dehydration on bromine loading in the upper troposphere and lower
441 stratosphere, *Atmos. Chem. Phys.*, 11, 2671–2687, doi:10.5194/acp-11-2671- 2011, 2011.
- 442 Aschmann, J., and Sinnhuber, B.-M.: Contribution of very short-lived substances to stratospheric
443 bromine loading: uncertainties and constraints, *Atmos. Chem. Phys.*, 13, 1203-1219,
444 doi:10.5194/acp-13-1203-2013, 2013.
- 445 Ashfold, M. J., Harris, N. R. P., Atlas, E. L., Manning, A. J., and Pyle, J. A.: Transport of short-
446 lived species into the Tropical Tropopause Layer, *Atmos. Chem. Phys.*, 12, 6309-6322,
447 doi:10.5194/acp-12-6309-2012, 2012.
- 448 Balkanski, Y. J., Jacob, D. J., Gardner, G. M., Graustein, W. C., and Turekian, K. K.: Transport
449 and residence times of tropospheric aerosols inferred from a global three-dimensional
450 simulation of ²¹⁰Pb, *J. Geophys. Res.*, 98, 20,573-20,586, doi:10.1029/93JD02456, 1993.
- 451 Blake, N. J., Blake, D. R., Simpson, I. J., Meinardi, S., Swanson, A. L., Lopez, J. P., Katzenstein,
452 A. S., Barletta, B., Shirai, T., Atlas, E., Sachse, G., Avery, M., Vay., S., Fuelberg, H. E.,
453 Kiley, C. M., Kita, K., Rowland, F. S.: NMHCs and halocarbons in Asian continental
454 outflow during the Transport and Chemical Evolution over the Pacific (TRACE-P) field
455 campaign: comparison with PEM-West B, *J. Geophys. Res.*, 108, 8806,
456 doi:10.1029/2002JD003367, 2003.
- 457 Brioude, J., Portmann, R. W., Daniel, J. S., Cooper, O. R., Frost, G. J., Rosenlof, K. H., Granier,
458 C., Ravishankara, A. R., Montzka, S. A. and Stohl, A.: Variations in ozone depletion
459 potentials of very short-lived substances with season and emission region." *Geophysical*
460 *Research Letters*, 37, L19804, doi:10.1029/2010GL044856, 2010.
- 461 Chin, M., Savoie, D. L., Huebert, B. J., Bandy, A. R., Thornton, D. C., Bates, T. S., Quinn, P. K.,
462 Saltzman, E. S., and De Bruyn, W. J.: Atmospheric sulfur cycle in the global model
463 GOCART: Comparison with field observations and regional budgets, *J. Geophys. Res.*, 105,
464 24 689–24 712, 2000.
- 465 Dorf, M., Bösch, H., Butz, A., Camy-Peyret, C., Chipperfield, M. P., Engel, A., Goutail, F.,
466 Grunow, K., Hendrick, F., Hrechanyy, S., Naujokat, B., Pommereau, J.-P.,
467 Van Roozendaal, M., Sioris, C., Stroh, F., Weidner, F., and Pfeilsticker, K.: Balloon-borne
468 stratospheric BrO measurements: comparison with Envisat/SCIAMACHY BrO limb profiles,
469 *Atmos. Chem. Phys.*, 6, 2483-2501, doi:10.5194/acp-6-2483-2006, 2006a.
- 470 Dorf, M., Butler, J. H., Butz, A., Camy-Peyret, C., Chipperfield, M. P., Kritten, L., Montzka, S.
471 A., Simmes, B., Weidner, F., and Pfeilsticke, K.: Long-term observations of stratospheric
472 bromine reveal slow down in growth, *Geophys. Res. Lett.*, 33, L24803,
473 doi:10.1029/2006GL027714, 2006b.
- 474 Dorf, M., Butz, A., Camy-Peyret, C., Chipperfield, M. P., Kritten, L., and Pfeilsticker, K.:
475 Bromine in the tropical troposphere and stratosphere as derived from balloon-borne BrO
476 observations, *Atmos. Chem. Phys.*, 8, 7265–7271, 2008.
- 477 Douglass, A. R. and Kawa, S. R.: Contrast between 1992 and 1997 high-latitude spring Halogen
478 Occultation Experiment observations of lower stratospheric HCl, *J. Geophys. Res.*,
479 104(D15), 18739–18754, doi:10.1029/1999JD900281, 1999.

480 Dvortsov, V. L., Geller, M. A., Solomon, S., Schauffler, S. M., Atlas, E. L., and Blake, D. R.:
481 Rethinking reactive halogen budgets in the midlatitudes lower stratosphere, *Geophys. Res.*
482 *Lett.*, 26, 1699–1702, 1999.

483 Fueglistaler, S., Wernli, J. and Peter, T.: Tropical troposphere-to-stratosphere transport inferred
484 from trajectory calculations, *J. Geophys. Res.*, 109, D03108, doi:10.1029/2003JD04069,
485 2004.

486 Fueglistaler, S., Dessler, A. E., Dunkerton, T. J., Folkins, I., Fu, Q., and Mote, P. W.: Tropical
487 tropopause layer, *Rev. Geophys.*, 47, 1, doi:10.1029/2008RG000267, 2009.

488 Gettelman, A., and Forster, P. M. D. F.: A climatology of the tropical tropopause layer, *J.*
489 *Meteorol. Soc. Jpn.*, 80, 911-924, 2002.

490 Ginoux, P., Chin, M., Tegen, I., Prospero, J., Holben, B., Dubovik, O., and Lin, S.-J.: Sources
491 and distributions of dust aerosols simulated with the GOCART model, *J. Geophys. Res.*, 106,
492 20 225–20 273, 2001.

493 Giorgi, F., and Chameides, W. L.: Rainout lifetimes of highly soluble aerosols and gases as
494 inferred from simulations with a general circulation model, *J. Geophys. Res.*, 91, 14,367-
495 14,376, 1986.

496 Hatsushika, H., and Yamazaki, K.: Stratospheric drain over Indonesia and dehydration within the
497 tropical tropopause layer diagnosed by air parcel trajectories, *J. Geophys. Res.*, 108(D19),
498 4610, doi:10.1029/2002JD002986, 2003.

499 Hossaini, R., Chipperfield, M. P., Monge-Sanz, B. M., Richards, N. A. D., Atlas, E., and Blake,
500 D. R.: Bromoform and dibromomethane in the tropics: a 3-D model study of chemistry and
501 transport, *Atmos. Chem. Phys.*, 10, 719-735, 2010.

502 Hossaini, R., Chipperfield, M. P., Feng, W., Breider, T. J., Atlas, E., Montzka, S. A., Miller, B.
503 R., Moore, F., and Elkins, J.: The contribution of natural and anthropogenic very short-lived
504 species to stratospheric bromine, *Atmos. Chem. Phys.*, 12, 371-380, doi:10.5194/acp-12-371-
505 2012, 2012a.

506 Hossaini, R., Chipperfield, M. P., Dhomse, S., Ordonez, C., Saiz-Lopez, A., Abraham, N. L.,
507 Archibald, A., Braesicke, P., Telford, P., Warwick, N., Yang, X. and Pyle, J.: Modelling
508 future changes to the stratospheric source gas injection of biogenic bromocarbons."
509 *Geophysical Research Letters*, 39, L20813, doi:10.1029/2012GL053401, 2012b.

510 Hossaini, R., Mantle, H., Chipperfield, M. P., Montzka, S. A., Hamer, P., Ziska, F., Quack, B.,
511 Krüger, K., Tegtmeier, S., Atlas, E., Sala, S., Engel, A., Bönisch, H., Keber, T., Oram, D.,
512 Mills, G., Ordóñez, C., Saiz-Lopez, A., Warwick, N., Liang, Q., Feng, W., Moore, F.,
513 Miller, B. R., Marécal, V., Richards, N. A. D., Dorf, M., and Pfeilsticker, K.: Evaluating
514 global emission inventories of biogenic bromocarbons, *Atmos. Chem. Phys. Discuss.*, 13,
515 12485-12539, doi:10.5194/acpd-13-12485-2013, 2013.

516 Hoyle, C. R., Marécal, V., Russo, M. R., Allen, G., Arteta, J., Chemel, C., Chipperfield, M. P.,
517 D'Amato, F., Dessens, O., Feng, W., Hamilton, J. F., Harris, N. R. P., Hosking, J. S.,
518 Lewis, A. C., Morgenstern, O., Peter, T., Pyle, J. A., Reddman, T., Richards, N. A. D.,
519 Telford, P. J., Tian, W., Viciani, S., Volz-Thomas, A., Wild, O., Yang, X., and Zeng, G.:
520 Representation of tropical deep convection in atmospheric models – Part 2: Tracer transport,
521 *Atmos. Chem. Phys.*, 11, 8103-8131, doi:10.5194/acp-11-8103-2011, 2011.

522 Kreygy, S., Camy-Peyret, C., Chipperfield, M. P., Dorf, M., Feng, W., Hossaini, R., Kritten, L.,
523 Werner, B., and Pfeilsticker, K.: Atmospheric test of the $J(\text{BrONO}_2)/k_{\text{BrO}+\text{NO}_2}$ ratio:
524 implications for total stratospheric Br_y and bromine-mediated ozone loss, *Atmos. Chem.*
525 *Phys.*, 13, 6263-6274, doi:10.5194/acp-13-6263-2013, 2013.

526 Kurylo, M. J., and Rodriguez, J. M.: Short-lived ozone related compounds, in Scientific
527 Assessment of Ozone Depletion: 1998, Global Ozone Res. and Monit. Proj., Rep. 44, chap.
528 2, World Meteorol. Organ., Geneva, Switzerland. 1999.

529 Levine, J. G., Braesicke, P., Harris, N. R. P., Savage, N. H., and Pyle, J. A.: Pathways and
530 timescales for troposphere-to-stratosphere transport via the tropical tropopause layer and
531 their relevance for very short lived substances, *J. Geophys. Res.*, 112,
532 doi:10.1029/2005JD006940, 2007.

533 Levine, J. G., Braesicke, P., Harris, N. R. P., Pyle, J. A.: Seasonal and inter-annual variations in
534 troposphere-to-stratosphere transport from the tropical tropopause layer, *Atmos. Chem. Phys.*
535 8, 3689-3703, 2008.

536 Liang, Q., Stolarski, R. S., Kawa, S. R., Nielsen, J. E., Douglass, A. R., Rodriguez, J. M.,
537 Blake, D. R., Atlas, E. L., and Ott, L. E.: Finding the missing stratospheric Bry: a global
538 modeling study of CHBr₃ and CH₂Br₂, *Atmos. Chem. Phys.*, 10, 2269-2286,
539 doi:10.5194/acp-10-2269-2010, 2010.

540 Lin, S.-J.: A “vertically Lagrangian” finite-volume dynamical core for global models, *Mon.*
541 *Weather Rev.*, 132(10), 2293–2307, 2004.

542 Liu, H., Jacob, D. J., Bey, I., and Yantosca, R. M.: Constraints from ²¹⁰Pb and ⁷Be on wet
543 deposition and transport in a global three-dimensional chemical tracer model driven by
544 assimilated meteorological fields, *J. Geophys. Res.*, 106(D11), 12109–12128,
545 doi:10.1029/2000JD900839, 2001.

546 Moorthi, S., and Suarez, M. J.: Relaxed Arakawa–Schubert: A parameterization of moist
547 convection for general circulation models, *Mon. Wea. Rev.*, 120, 978–1002, 1992.

548 Nielsen, J. E., and Douglass A. R.: A simulation of bromoform’s contribution to stratospheric
549 bromine, *J. Geophys. Res.*, 106, 8089– 8100, 2001.

550 Ordóñez, C., Lamarque, J.-F., Tilmes, S., Kinnison, D. E., Atlas, E. L., Blake, D. R.,
551 Sousa Santos, G., Brasseur, G., and Saiz-Lopez, A.: Bromine and iodine chemistry in a
552 global chemistry-climate model: description and evaluation of very short-lived oceanic
553 sources, *Atmos. Chem. Phys.*, 12, 1423-1447, doi:10.5194/acp-12-1423-2012, 2012.

554 Ott, L. E., Bacmeister, J., Pawson, S., Pickering, K., Stenchikov, G., Suarez, M. Huntriester, H.,
555 Loewenstein, M., Lopez, J., and Xueref-Remy, I.: Analysis of Convective Transport and
556 Parameter Sensitivity in a Single Column Version of the Goddard Earth Observation System,
557 Version 5, General Circulation Model. *J. Atmos. Sci.*, **66**, 627–646, 2009.

558 Ott, L. E., Pawson, S., and Bacmeister, J.: An analysis of the impact of convective parameter
559 sensitivity on simulated global atmospheric CO distributions, *J. Geophys. Res.* 116, D21310,
560 doi:10.1029/2011JD016077, 2011.

561 Parrella, J. P., Jacob, D. J., Liang, Q., Zhang, Y., Mickley, L. J., Miller, B., Evans, M. J., Yang,
562 X., Pyle, J. A., Theys, N., and Van Roozendaal, M., *Atmos. Chem. Phys.*, 12, 6723-6720,
563 doi:10.5194/acp-12-6723-2012, 2012.

564 Pyle, J. A., Ashfold, M. J., Harris, N. R. P., Robinson, A. D., Warwick, N. J., Carver, G. D.,
565 Gostlow, B., O'Brien, L. M., Manning, A. J., Phang, S. M., Yong, S. E., Leong, K. P.,
566 Ung, E. H., and Ong, S.: Bromoform in the tropical boundary layer of the Maritime
567 Continent during OP3, *Atmos. Chem. Phys.*, 11, 529-542, doi:10.5194/acp-11-529-2011,
568 2011.

569 Randel, W. J., and Jensen, E. J.: Physical processes in the tropical tropopause layer and their role
570 in a changing climate, *Nature Geoscience*, 6, 169-176, doi:10.1038/ngeo1733, 2013.

571 Reinecker, M. M, Suarez, M. J., Todling, R., Bacmeister, J., Takacs, L., Liu, H.-C., Gu, W.,
572 Sienkiewicz, M., Koster, R. D., Gelaro, R., Stajner, I., and Nielsen, J. E.: The GEOS-5 Data
573 Assimilation System-Documentation of Versions 5.0.1, 5.1.0, and 5.2.0, Tech. Rep. 104606
574 V27, NASA, Greenbelt, MD, 2008.

575 Rozanov, A., Köhl, S., Doicu, A., McLinden, C., Puķite, J., Bovensmann, H., Burrows, J. P.,
576 Deutschmann, T., Dorf, M., Goutail, F., Grunow, K., Hendrick, F., von Hobe, M.,
577 Hrechanyy, S., Lichtenberg, G., Pfeilsticker, K., Pommereau, J. P., Van Roozendael, M.,
578 Stroh, F., and Wagner, T.: BrO vertical distributions from SCIAMACHY limb
579 measurements: comparison of algorithms and retrieval results, *Atmos. Meas. Tech.*, 4, 1319-
580 1359, doi:10.5194/amt-4-1319-2011, 2011.

581 Sander, S. P., Abbatt, J. P. D., Barker, J. R., Burkholder, J. B., Golden, D. M., Kolb, C. E.,
582 Kurylo, M. J., Moortgat, G. K., Wine, P. H., Huie, R. E., Orkin, V. L.: Chemical Kinetics and
583 Photochemical Data for Use in Atmospheric Studies: Evaluation No. 17, JPL Publ. 10-6, Jet
584 Propul. Lab., Pasadena, CA, USA, 2011.

585 Salawitch, R. J., Canty, T., Kurosu, T., Chance, K., Liang, Q., da Silva, A., Pawson, S., Nielsen,
586 J. E., Rodriguez, J. M., Bhartia, P. K., Liu, X., Huey, L. G., Liao, J., Stickel, R. E., Tanner,
587 D. J., Dibb, J. E., Simpson, W. R., Donohoue, D., Weinheimer, A., Flocke, F., Knapp, D.,
588 Montzka, D., Neuman, J. A., Nowak, J. B., Ryerson, T. B., Oltmans, S., Blake, D. R., Atlas,
589 E. L., Kinnison, D. E., Tilmes, S., Pan, L. L., Hendrick, F., Van Roozendael, M., Kreher, K.,
590 Johnston, P. V., Gao, R. S., Johnson, B., Bui, T. P., Chen, G., Pierce, R. B., Crawford, J. H.,
591 and Jacob, D. J.: A new interpretation of total column BrO during Arctic spring, *Geophys.*
592 *Res. Lett.*, 37, L21805, doi:10.1029/2010GL043798, 2010.

593 Schauffler, S. M., Atlas, E. L., Blake, D. R., Flocke, F., Lueb, R. A., Lee-Taylor, J. M., Stroud,
594 V., and Travnicek, W.: Distributions of brominated organic compounds in the troposphere
595 and lower stratosphere, *J. Geophys. Res.*, 104 (D17), 21513-21535, 1999.

596 Sinnhuber, B.-M., Rozanov, A., Sheode, N., Afe, O. T., Richter, A., Sinnhuber, M., Wittrock, F.,
597 Burrows, J. P., Stiller, G.P., von Clarmann, T., and Linden, A.: Global observations of
598 stratospheric bromine monoxide from SCIAMACHY, *Geophys. Res. Lett.*, 32, L20810, doi:
599 10.1029/2005GL023839, 2005.

600 Sinnhuber, B.-M. and Folkins, I.: Estimating the contribution of bromoform to stratospheric
601 bromine and its relation to dehydration in the tropical tropopause layer, *Atmos. Chem. Phys.*,
602 6, 4755–4761, 2006.

603 Sioris, C.E., Kovalenko, L. J., McLinden, et al.: Latitudinal and vertical distribution of bromine
604 monoxide in the lower stratosphere from Scanning Imaging Absorption Spectrometer for
605 Atmospheric Chartography limb scattering measurements, *J. Geophys. Res.*, 111, D14301,
606 doi: 10.1029/2005JD006479, 2006.

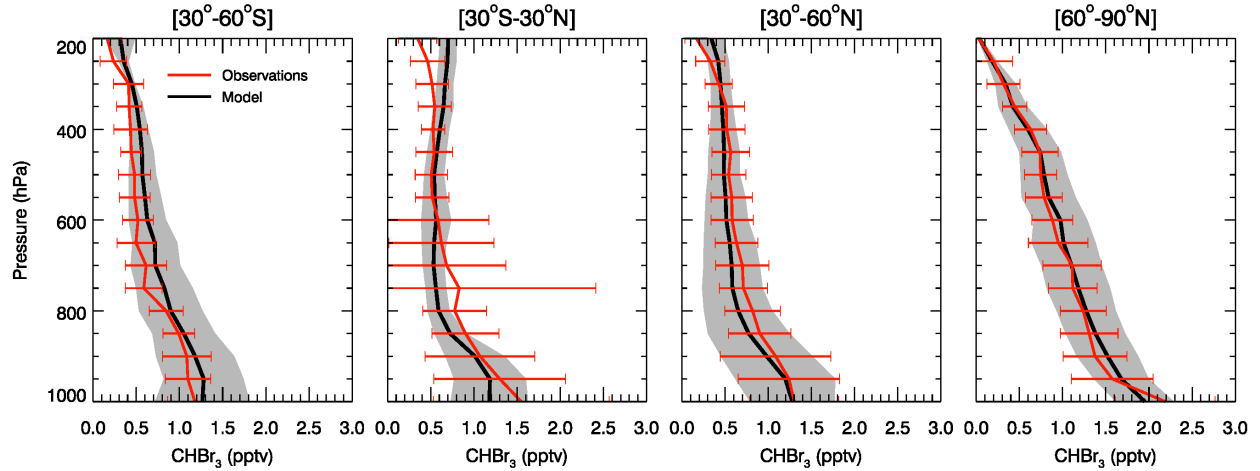
607 Spivakovsky, C. M., Logan, J. A., Montzka, S. A., Balkanski, Y. J., M. Foreman-Fowler, ones,
608 D. B. A., Horowitz, L. W., Fusco, A. C., Brenninkmeijer, C. A. M., Prather, M. J., Wofsy, S.
609 C., and McElroy, M. B.: Three-dimensional climatological distribution of tropospheric OH:
610 Update and evaluation, *J. Geophys. Res.*, 105, 8931–8980, 2000.

611 Sturges, W.T., Oram, D. E., Carpenter, L. J., Penkett, S. A. and Engel, A.: Bromoform as a
612 source of stratospheric bromine, *Geophys. Res. Lett.*, 27 (14), 2081-2084, 2000.

613 Warwick, N. J., Pyle, J. A., Carver, G. D., Yang, X., Savage, N. H., O’Connor, F. M., and Cox,
614 R. A.: Global modeling of biogenic bromocarbons, *J. Geophys. Res.*, 111, D24305,
615 doi:10.1029/2006JD007264, 2006.

616 Webster, P. J.: The large scale structure of the tropical atmosphere, *General Circulation of the*

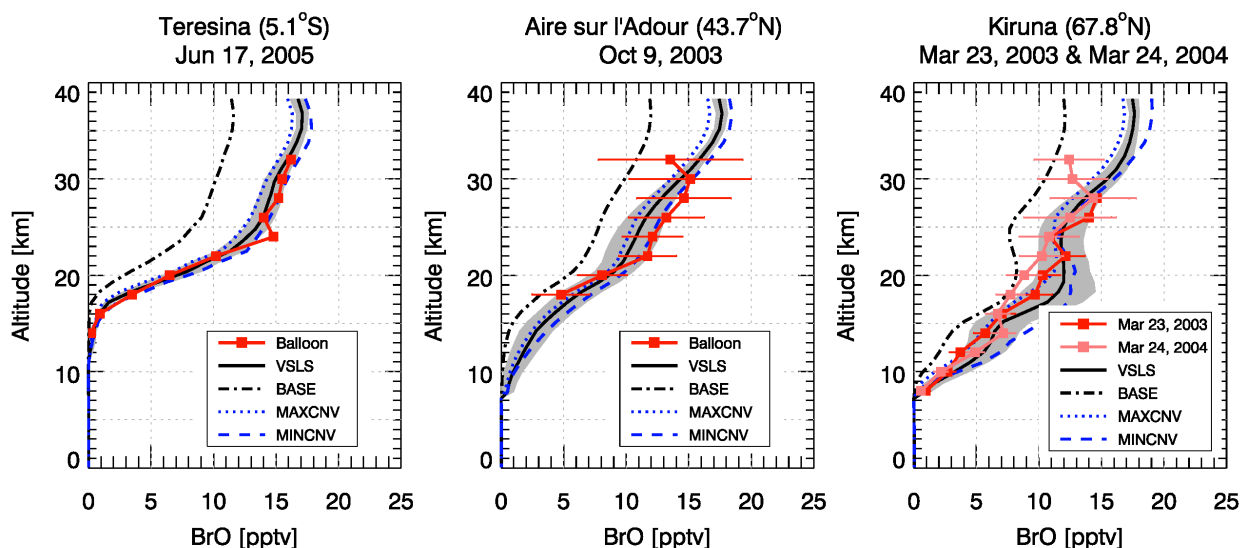
617 Atmosphere, Academic Press, pp. 235-275, 1983.
618 WMO (2011), *Scientific Assessment of Ozone Depletion: 2010, Global Ozone Research and*
619 *Monitoring Project-Report No. 52*, 516 pp., Geneva, Switzerland.
620 Yang, X., Cox, R. A., Warwick, N. J., Pyle, J. A., Carver, G. D., and O'Connor F. M.:
621 Tropospheric bromine chemistry and its impacts on ozone: A model study, *J. Geophys. Res.*,
622 110, D23311, doi: 10.1029/2005-JD006244, 2005.
623 Ziska, F., Quack, B., Abrahamsson, K., Archer, S. D., Atlas, E., Bell, T., Butler, J. H.,
624 Carpenter, L. J., Jones, C. E., Harris, N. R. P., Hepach, H., Heumann, K. G., Hughes, C.,
625 Kuss, J., Krüger, K., Liss, P., Moore, R. M., Orlikowska, A., Raimund, S., Reeves, C. E.,
626 Reifenhäuser, W., Robinson, A. D., Schall, C., Tanhua, T., Tegtmeier, S., Turner, S.,
627 Wang, L., Wallace, D., Williams, J., Yamamoto, H., Yvon-Lewis, S., and Yokouchi, Y.:
628 Global sea-to-air flux climatology for bromoform, dibromomethane and methyl iodide,
629 *Atmos. Chem. Phys.*, 13, 8915-8934, doi:10.5194/acp-13-8915-2013, 2013.
630
631
632



632
 633
 634
 635
 636
 637
 638
 639
 640
 641

Figure 1. Comparison between the observed (red lines with horizontal bars indicating one standard deviation) and simulated (black lines with gray shading showing one sigma variability) vertical profiles of CHBr₃ in the troposphere. Observations are compiled using Whole Air Sampler canister measurements from eight NASA aircraft missions are averaged for 30-60°S, 30°S-30°N, 30-60°N, and 60-90°N latitude bands at 1-km vertical interval. Model is sampled at the same location as the observations in the corresponding month in 2010.

641



642

643

644

645

646

647

648

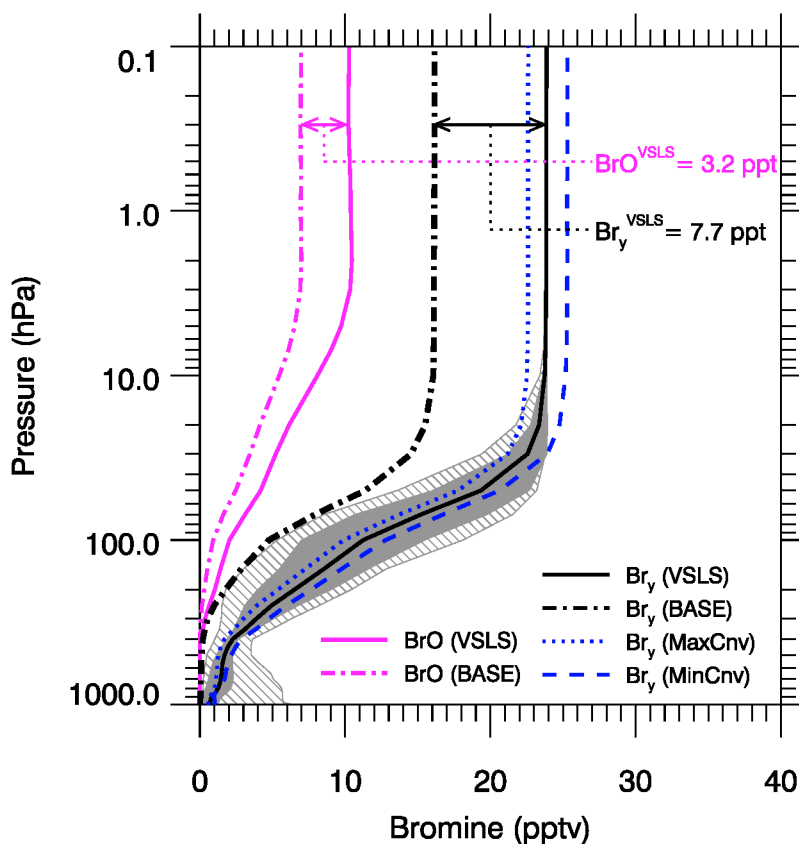
649

650

651

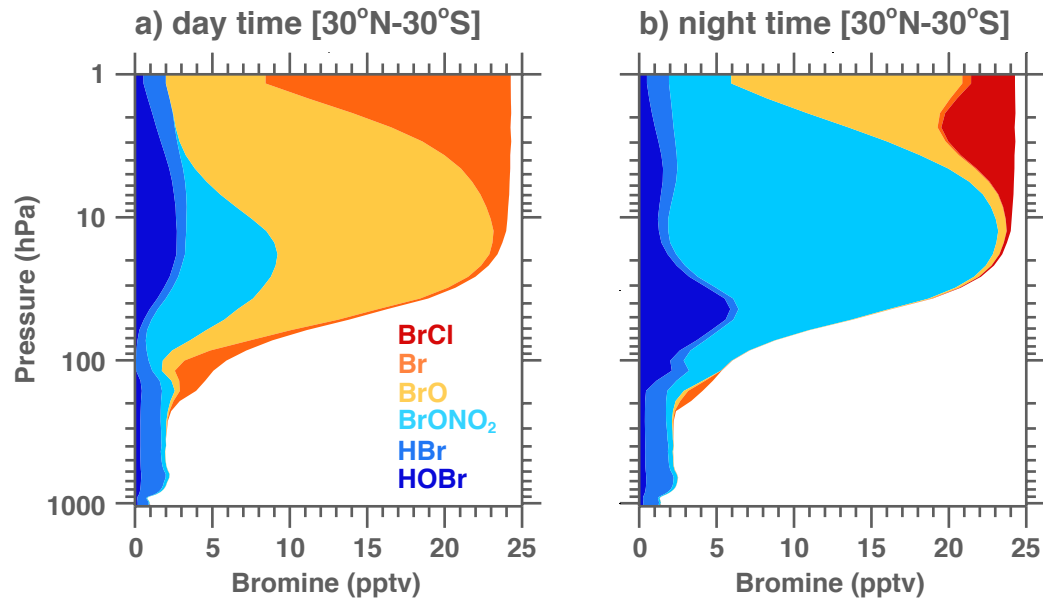
652

Figure 2. Comparison of simulated BrO from the GEOSCCM run R_{VLSL} (black solid line with 1-sigma variance in gray shading) with balloon measurements (red line with 1-sigma uncertainty in horizontal bars) from the LPMA/DOAS Spectrometers in the stratosphere. The black dash-dotted line shows simulated BrO from the run without VLSL (R_{BASE}). Simulated BrO from the two convective sensitivity simulations are also shown (dotted line for maximum convection condition and dashed line for minimum convection condition). The model is sampled at the same month and latitude as the balloon measurements but only daytime profiles from all available longitude grid points are collected to calculate the 1-sigma variance of simulated BrO.



653
 654
 655
 656
 657
 658
 659
 660
 661

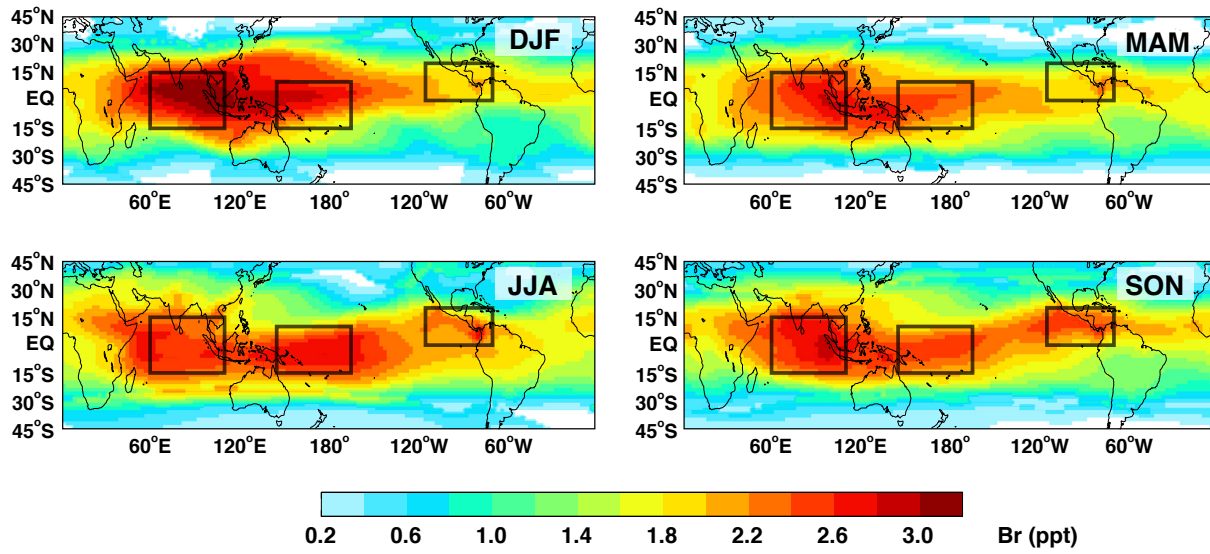
Figure 3. Model simulated global and annual mean BrO and Br_y profiles from the simulation with VLSL (R_{VLSL} , solid lines) and the base simulation without VLSL (R_{BASE} , dash-dotted lines) for Year 2010. The gray shadings indicate the spread of annual mean Br_y in the R_{VLSL} run with the hatched areas indicate the minimum to maximum range and the filled shadings indicate 1-sigma variance. Br_y from the two convective sensitivity simulations are also shown (blue dashed and dotted line for minimum and maximum convection conditions, respectively).



662
 663
 664
 665
 666

Figure 4. Annual mean model inorganic bromine (BrCl, Br, BrO, BrONO₂, HBr, HOBr) tropical vertical profiles for daytime (left panel) and nighttime (right panel), averaged between 30°N-30°S.

667



668

669

670

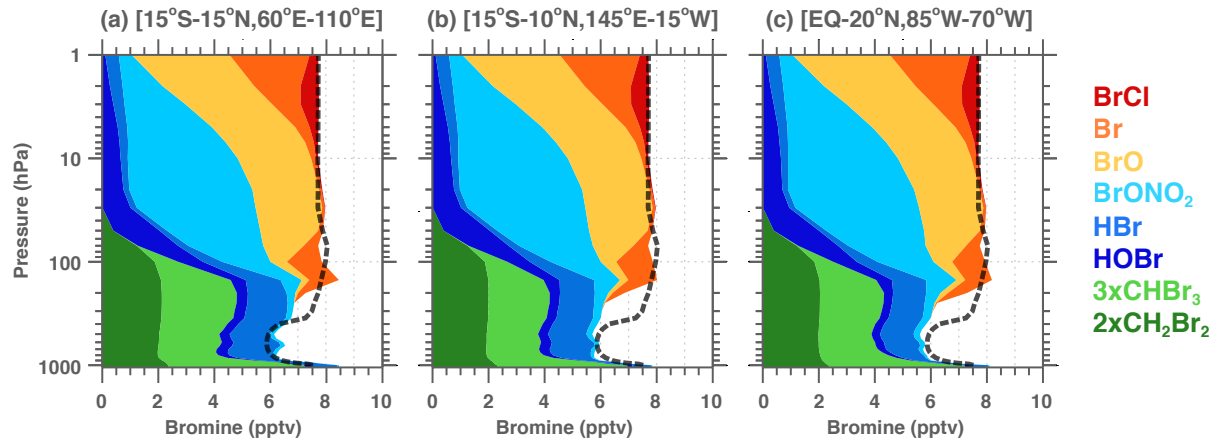
671

672

673

674

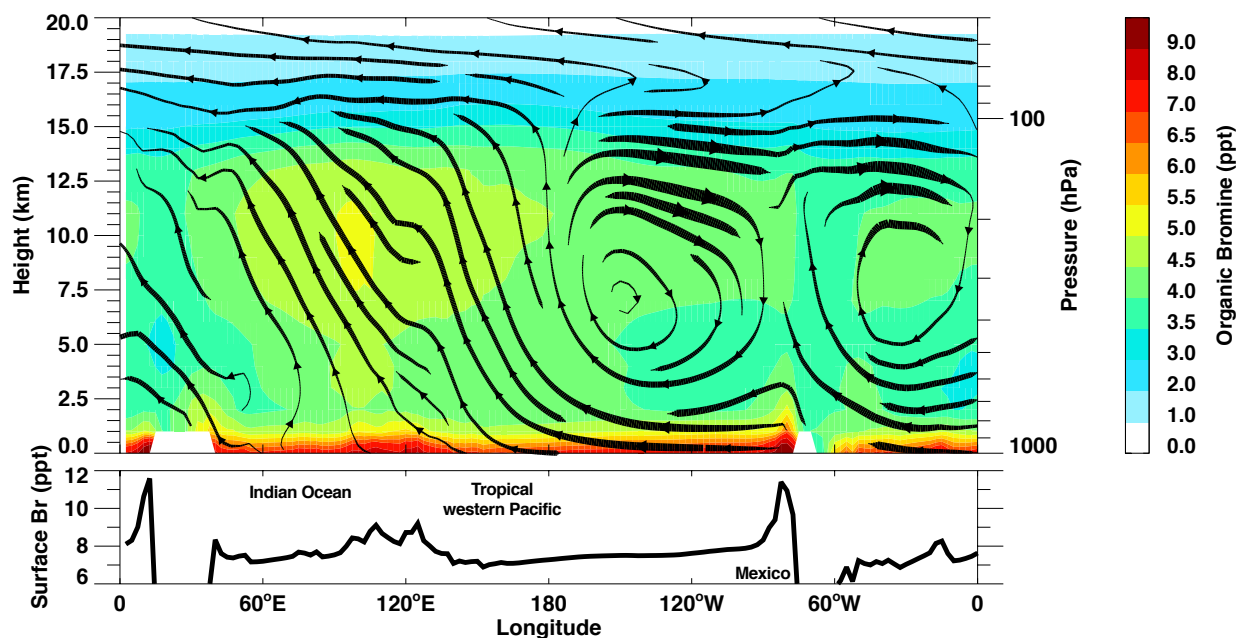
Figure 5. 10-year averaged (2001-2010) seasonal mean distribution of simulated CHBr₃ (unit ppt Br) at the 355K potential temperature layer (just below tropopause) in DJF, MAM, JJA and SON. The black boxes outline the three regions where most active troposphere-to-stratosphere transport occurs.



674
 675
 676
 677
 678
 679
 680
 681
 682
 683

Figure 6. The contribution of organic bromine ($\text{CH}_2\text{Br}_2 \times 2$, $\text{CHBr}_3 \times 3$) and inorganic bromine (Br_y^{VLS}) from CHBr_3 and CH_2Br_2 degradation to atmospheric bromine in three active TST regions (a) the tropical Indian Ocean (left), (b) the tropical western Pacific warm pool (middle), and (c) the Pacific Coast of Mexico (right). The soluble product gases (HBr, HOBr, BrONO_2) and insoluble product gases (Br, BrO, BrCl) are shown in blue colors and warm colors, respectively. The global mean sum of organic and inorganic bromine from VLS is also shown (thick black dashed line). The model results are 10-year annual averages from 2001-2010.

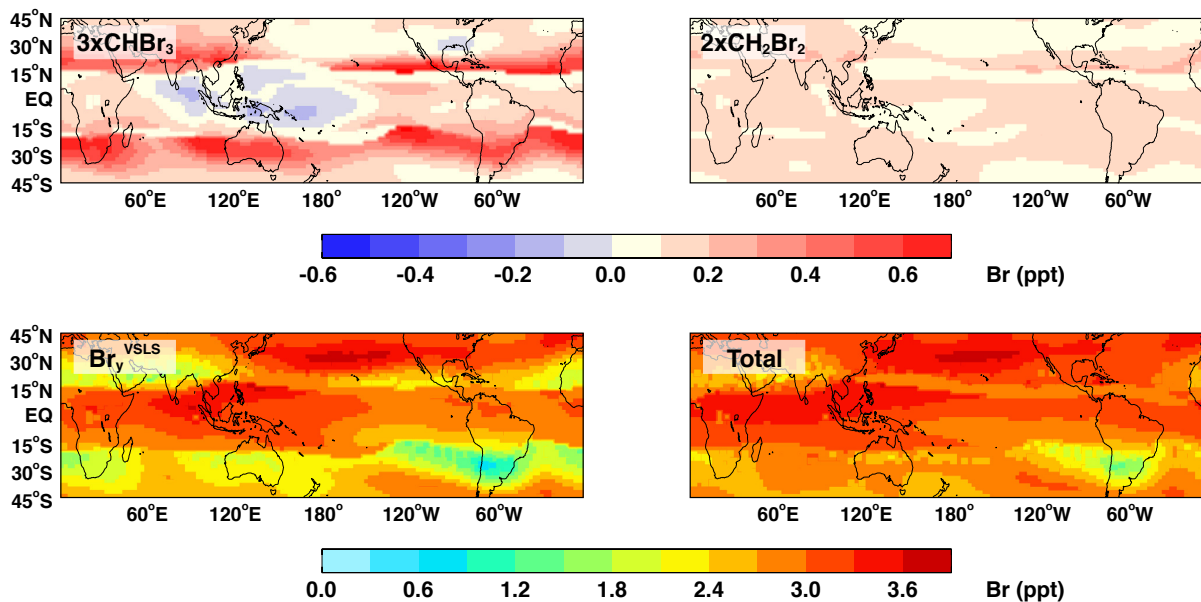
683



684
685
686
687
688
689

Figure 7. Longitude-height cross-section of modeled total VSL organic bromine ($\text{CHBr}_3 \times 3 + \text{CH}_2\text{Br}_2 \times 2$) (color contours) and streamlines (black lines) in the deep tropics. The organic bromine and wind streams are 10-year annual averages (2001-2010) between 10°S - 10°N . Surface organic bromine abundance is shown as the black solid line at the bottom panel.

MinCnv - MaxCnv: 355K - 380K



689
690
691
692
693

Figure 8. The simulated annual mean difference between the R_{MINCNV} and R_{MAXRUN} runs in organic bromine (3xCHBr₃, 2xCH₂Br₂), inorganic bromine and total bromine from VSLs between 355-380K. The model results are 10-year annual averages from 2001-2010.